TISSUE ENGINEERING: Part A
Volume 17, Numbers 5 and 6, 2011

DOI: 10.1089/ten.tea.2010.0298

Engineered Pullulan–Collagen Composite Dermal Hydrogels Improve Early Cutaneous Wound Healing

Victor W. Wong, M.D., Kristine C. Rustad, B.S., Michael G. Galvez, B.A., Evgenios Neofytou, M.D., Jason P. Glotzbach, M.D., Michael Januszyk, M.D., Melanie R. Major, Michael Sorkin, M.D., Michael T. Longaker, M.D., M.B.A., Jayakumar Rajadas, Ph.D., and Geoffrey C. Gurtner, M.D.

New strategies for skin regeneration are needed to address the significant medical burden caused by cutaneous wounds and disease. In this study, pullulan–collagen composite hydrogel matrices were fabricated using a salt-induced phase inversion technique, resulting in a structured yet soft scaffold for skin engineering. Salt crystallization induced interconnected pore formation, and modification of collagen concentration permitted regulation of scaffold pore size. Hydrogel architecture recapitulated the reticular distribution of human dermal matrix while maintaining flexible properties essential for skin applications. *In vitro*, collagen hydrogel scaffolds retained their open porous architecture and viably sustained human fibroblasts and murine mesenchymal stem cells and endothelial cells. *In vivo*, hydrogel-treated murine excisional wounds demonstrated improved wound closure, which was associated with increased recruitment of stromal cells and formation of vascularized granulation tissue. In conclusion, salt-induced phase inversion techniques can be used to create modifiable pullulan–collagen composite dermal scaffolds that augment early wound healing. These novel biomatrices can potentially serve as a structured delivery template for cells and biomolecules in regenerative skin applications.

Introduction

Skin engineering requires biomaterials capable of recapitulating the structural architecture of unwounded skin, which is irreversibly destroyed by injury or disease.[1] This organized structure is normally provided by the extracellular matrix (ECM), a complex scaffold that supports and regulates the myriad cell types involved in skin homeostasis.[2] Dermal scaffolds, derived from both native and synthetic sources, can serve as the structural template during repair and have been used clinically for skin replacement.[1,3] However, native dermal sources such as decellularized cadaveric skin are limited by cost, donor availability, and disease transmission concerns.[4,5] Alternatively, synthetic matrices are potentially affordable, modifiable, and widely available dermal substitutes that can be used for skin engineering[6] but are generally accepted as being inferior to allogeneic tissue. This may be because of the inability of engineered matrices to accurately replicate the architecture of unwounded dermis.

The dermal ECM consists mostly of type I collagen fibers arranged in a reticular fashion. The structural organization of collagen determines its functional diversity in tissues as different as bone and skin.[7] Although hard collagen scaffolds have been used extensively in bone and cartilage engineering, options for soft collagen scaffolds are limited owing to the difficulties of maintaining structure in a nonrigid environment.[8] One strategy to achieve three-dimensional organization in a soft biomaterial involves hydrogel systems, which have been fabricated from polymeric substrates such as alginate, hyaluronic acid, and polyethylene glycol,[9–12] and ECM components including collagen, elastin, and fibrin.[13–15] Hydrogels have previously been utilized as scaffolds, gels, films, and foams for a wide range of skin applications,[10] but properties suitable for wound coverage or treating infection are not necessarily ideal for skin engineering and dermal reconstruction. Specifically, existing hydrogel systems excel at providing inductive cues but generally lack important structural contexts for *in situ* skin repair. An ideal hydrogel system would provide both form and function to promote skin regeneration following injury.

One promising biomaterial for dermal hydrogel fabrication is pullulan, a linear homopolysaccharide produced by the fungus *Aureobasidium pullulans*. It has been increasingly studied as a biomaterial scaffold given its biodegradable, nontoxic, and modifiable nature.[16,17] This unique carbohydrate exhibits water retention capabilities ideal for hydrogel-based delivery of both cells and biomolecules[18] and contains multiple functional groups which permit crosslinking and

Department of Surgery, Stanford University School of Medicine, Stanford, California.

delivery of genetic material and therapeutic cytokines.[19,20] Additionally, smooth muscle cells and endothelial progenitor cells have been sustained within pullulan-based hydrogels *in vitro*,[21,22] demonstrating their potential to facilitate cell-based dermal replacement strategies.

Expensive and complex processing techniques such as gas foaming, cryogenic processes, electrospinning, and powder sintering have been used to construct rigid porous scaffolds.[23–25] On the other hand, simpler techniques such as salt-induced phase inversion and leaching have been used to create effective biomatrices with minimal use of sophisticated equipment.[26–28] In this study, we aimed to fabricate dermal-like pullulan–collagen hydrogels using a novel salt-induced phase inversion technique. The aim was to create a modifiable dermal scaffold that recapitulates the structural environment of unwounded skin to improve wound healing.

Materials and Methods

Materials

Carbohydrate-based hydrogels were fabricated using pullulan (molecular weight 200,000; Hayashibara Laboratories, Okayama, Japan). Collagen was prepared from rat tail collagen type I solution (Sigma-Aldrich, St. Louis, MO). Crosslinking was performed with sodium trimetaphosphate (STMP; Sigma-Aldrich) under alkaline conditions with sodium hydroxide (Sigma-Aldrich). Potassium chloride salt (KCl; Sigma-Aldrich) was used as a porogen for in-gel crystallization. Ninety-five percent ethyl alcohol (Sigma-Aldrich) was used for hydrogel dehydration. Pullulanase (Sigma-Aldrich) was prepared in a concentration of 4 U/mL in phosphate-buffered saline (PBS) (Gibco, Grand Island, NY). Collagenase A (from *Clostridium histolyticum*, >0.15 Wünsch units/mg—one Wünsch unit liberates 1 μM of 4-phenylazobenzyloxycarbonyl-L-prolyl-L-leucine formed in 1 min at 25°C at pH 7.1 from 4-phenylazobenzyloxycarbonyl-L-prolyl-L-leucyl-glycyl-L-prolyl-D-arginine substrate[29]; Roche, Indianapolis, IN) was prepared in a concentration of 2 mg/mL in PBS. Methylene blue (Sigma-Aldrich) was used to quantify STMP crosslinking based on previously published methods.[30,31] All aqueous solutions were prepared in Milli-Q water (Millipore, Billerica, MA). All other compounds and reagents were used without further purification.

Cells and animals

Ten- to 12-week-old male C57BL/6 mice (Jackson Laboratories, Bar Harbor, ME) were used for bone-marrow-derived mesenchymal stem cell (MSC) harvest, subcutaneous hydrogel implantation ($n = 12$), and excisional wound model experiments ($n = 10$). Mice were fed *ad libitum* water and rodent chow, and housed in the Stanford University animal facility under institution-approved guidelines.

Murine MSCs were harvested as previously described.[32] Fibroblasts (passage 3) were obtained from a primary line of human foreskin fibroblasts. bEnd.3 endothelial cells were obtained from American Type Culture Collection (Manassas, VA). Cells were maintained in Dulbecco's modified Eagle's medium (4.5 g/mL glucose; Gibco) supplemented with 10% fetal bovine serum (v/v) (Gibco) and 1% penicillin/streptomycin (Gibco).

Hydrogel fabrication

On the basis of previously published methods,[21] 2 g of pullulan powder was mixed with 2 g of STMP and 2 g KCl in 50 mg NaOH dissolved in deionized H_2O with or without collagen to a total volume of 10 mL. Collagen was mixed in at a concentration of 0%, 5%, or 10% of the weight of pullulan (0, 0.1, and 0.2 g collagen per 2 g pullulan, respectively). The composite mixture was gently vortexed for 30 min at 4°C to promote the homogeneous distribution of polymers within the hydrogel. The mixture was then poured onto Teflon sheets and compressed to create 2-mm-thick films. Hydrogel films were then dehydrated in 100% ethyl alcohol for 15 min and allowed to dry overnight. Dried films were washed in PBS at room temperature until the wash pH was 7.0 and stored at 4°C until further use. Six-millimeter punch biopsy disks of 2 mm thickness were used for all experiments. Films were sterilized overnight under UV light prior to all experiments.

Swelling property

Hydrogel water absorption capacity was calculated as a swelling ratio (grams liquid/grams protein):

$$\text{Swelling ratio} = (\text{weight of wet sample} - \text{weight of dry sample})/\text{weight of dry sample}$$

For incubation studies, 5% collagen–pullulan hydrogels were incubated in deionized water or in PBS at 4°C or 37°C. Excess liquid was gently shaken off and weights of swollen gels were obtained. Hydrogel weights were measured at 12, 24, 48, and 72 h. Six samples were tested for each condition.

Scanning electron microscopy

Hydrogel imaging with variable pressure scanning electron microscopy (SEM) has been previously described.[33,34] Briefly, hydrogel samples and acellular human dermal matrix (DermaMatrix; Synthes, West Chester, PA) were incubated overnight in PBS, mounted onto adhesive carbon film on 15 mm aluminum stubs, and sputter-coated with 100Å gold/palladium using a Denton Desk II TSC Sputter Coater (Denton Vacuum, Moorestown, NJ). The samples were observed using a Hitachi S-3400N VP-SEM (Hitachi Ltd., Pleasanton, CA) operated at 10–15 kV with a working distance 8–10 mm and secondary electron detection. Hydrated hydrogels were mounted onto 10 mm stubs fitting a Deben Peltier cool stage (Deben, Suffolk, England) set at 4°C inside the specimen chamber of a Hitachi S-3400N VP-SEM. The variable-pressure SEM allowed observation of nonconductive samples in their natural state, eliminating the need for sample preparation. To limit water loss, pressure and temperature were correlatively decreased until a chamber pressure of 60 Pa and stage temperature of −25°C were reached. Saturated water vapor at 60 Pa is correlated with a sublimation temperature of −25°C so that minimal freezing or moisture loss would occur under these conditions.[33] Backscattered electron detection was used to capture images at 15 kV, at a working distance of 8–10 mm.

For *in vitro* cellular incorporation studies, fibroblasts and MSCs were seeded via dropwise addition of 1×10^5 cells in 50 μL of cell media onto each 5% collagen–pullulan hydrogel disk and were incubated in cell culture media for 72 h. Scaffold/cell samples were fixed for 24 h at 4°C with 4%

paraformaldehye and 2% glutaraldehyde in 1 N sodium cacodylate buffer pH 7.3 (Electron Microscopy Sciences, Hatfield, PA). Fixed samples were washed in the same buffer, and postfixed for 1 h in 1% aqueous osmium tetroxide, washed in Milli-Q water, and observed with backscattered electron as described above. Ten random SEM fields were examined at low magnification to assess consistency of porosity. Pore size was calculated from 10 random pores from 10 high-power SEM fields using ImageJ software (National Institutes of Health, Bethesda, MD). Porosity was measured from 10 high-power SEM fields for each condition using the threshold function and area measurement tool in ImageJ. Pseudocolored SEM images were created with Adobe Photoshop CS3 (Adobe Systems Incorporated, San Jose, CA).

Network extraction analysis

Scanning micrographs of 0%, 5%, and 10% collagen–pullulan hydrogels were obtained at 400×magnification. Reference images were obtained from 400×scanning micrographs of acellular human dermal matrix (DermaMatrix; Synthes). A network extraction algorithm[35,36] was applied to high-resolution scanning electron micrographs. Briefly, images were smoothed with a low-pass Gaussian filter and binarized to reduce background signal. Network geometry was then extracted based on fiber size, length, orientation angle, and crosslinking to create quantifiable metrics for comparison of different biomatrices. Graphs were generated using MATLAB (The MathWorks, El Segundo, CA).

In vitro *degradation*

Dry 5% collagen–pullulan hydrogels were incubated with pullulanase (4 U/mL) in PBS and weighed every 30 min. Similar experiments were performed with collagenase A (2 mg/mL in PBS). Enzyme doses were based on published methods.[21,37,38] Combination degradation studies using both pullulanase and collagenase A were conducted in PBS using the same concentrations as above. The initial weight at time 0 was the dry weight and wet weights were used for subsequent measurements. Experiments were performed six times for each condition at room temperature.

Quantification of crosslinking

Methylene blue absorption shows a linear relationship with STMP crosslinking density.[30] Hydrogel mixtures containing pullulan only, collagen only, 5% collagen with pullulan, 5% collagen with STMP, pullulan with STMP, and 5% collagen–pullulan with STMP were incubated overnight with methylene blue. As a control, individual materials were used in the same absolute quantities as when used to fabricate 5% collagen–pullulan hydrogels. Initial absorption of methylene blue was recorded at 665 nm (A_0) preincubation and after overnight incubation (A). Results were normalized with dry preincubation hydrogel weight (Wt) in milligrams. Four samples were tested for each condition. A methylene blue absorption index (AI_{MB}) was calculated based on modification of a previously published equation[30]:

$$AI_{MB} = [(A_0 - A)/Wt] \times 1000$$

Scaffold AI_{MB} was calculated using the following equation:

$$\text{Scaffold } AI_{MB} = AI_{MB} \text{ for 0 \% collagen with no STMP} - AI_{MB} \text{ for sample}$$

In vitro *viability*

The ability of 5% collagen–pullulan hydrogel scaffolds to support cellular survival *in vitro* was assessed. Fibroblasts, MSCs, and endothelial cells were separately incubated with hydrogels for up to 7 days. Cells were seeded via dropwise addition of 1×10^5 cells in 50 μL of cell media to each scaffold. Cell-seeded scaffolds were incubated for 3 h in a 5% CO_2 incubator at 37°C. Cellular morphology was assessed daily and cellular survival was assessed with a live/dead assay (Calbiochem, Gibbstown, NJ) per manufacturer's instructions. Images were obtained with fluorescence microscopy (Zeiss Axioplan 2 Imaging; Carl Zeiss, Inc. Thornwood, NY) with band-pass filters set to detect FITC and rhodamine. Identical high-power field images obtained from different lasers were merged using Adobe Photoshop CS3 to create single images of red and green coexcitation. Live cells stained green, whereas only dead cells stained red. Cell counts of at least 20 cells per high-power field were taken from five random fields for each cell type.

Subcutaneous implantation

Wild-type adult mice ($n = 12$) were anesthetized with inhalational isoflurane. After cleansing with 70% alcohol, three 1 cm full-thickness transverse incisions separated by 2 cm were made on the shaved dorsum of wild-type mice. After overnight PBS incubation under UV light, 5% collagen–pullulan hydrogels were implanted subcutaneously and incisions were closed with 6-0 nylon suture (Ethicon, Somerville, NJ) and covered with a sterile occlusive dressing (Tegaderm; 3M, St. Paul, MN). Sutures were removed on postincision day 2. Wounds were examined daily and harvested at 3, 7, 14, and 21 days. Digital photographs were taken to quantify residual hydrogel size ($n = 3$ wounds for each condition).

Stented excisional wound model

As per previously published methods,[39] a stented excisional wound model was utilized to assess the effects of the 5% collagen hydrogel scaffold on wound repair. Briefly, silicone rings that circumscribe the excisional wound are sutured to the skin with 6-0 nylon, thus preventing wound contracture (primary means of rodent wound healing) and allowing the wound to close by both re-epithelialization and granulation tissue formation (similar to human wound healing). Scaffold disks were sterilized under UV light in PBS and then placed into excisional wounds and covered with Tegaderm. Control wounds did not have any material implanted. Digital photographs of the wounds were taken every other day during dressing changes and quantified using ImageJ. Results were evaluated by two blinded investigators ($n = 10$ wounds for each condition).

Microscopic analyses

Harvested tissue was briefly rinsed in PBS, embedded in TissueTek OCT compound (Sakura Finetek USA, Inc., Torrance, CA), frozen overnight at −80°C, and stored at −20°C until further processing. Frozen sections were cut at 8 μm thickness and mounted onto Superfrost/Plus glass slides

(Fisher Scientific, Pittsburgh, PA). Slides were then fixed in 4% paraformaldehyde and then allowed to air-dry. Sections were stained with hematoxylin and eosin (Sigma-Aldrich), Masson's trichrome (Sigma-Aldrich), or picrosirius red (Sigma-Aldrich). To confirm collagen content and distribution, hydrogels were imaged under polarized light. When viewed under circularly polarized light, collagen fibers exhibit bright birefringence when unstained and red-orange birefringence when stained with picrosirius red.[40,41] Collagen 1-specific immunofluorescence was performed using rabbit anti-rat collagen1 antibody (Abcam, Inc. Cambridge, MA) and goat anti-rabbit AlexaFluor 488 (Molecular Probes, Invitrogen, Carlsbad, CA). Capillaries were quantified by counting luminal structures containing red blood cells at 630× magnification.

Flow cytometric analysis

On postinjury day 3, untreated wounds and hydrogel-treated wounds were excised and digested for 1 h in Liberase TL (0.5 mg/mL; Roche) at 37°C. Single-cell suspensions were filtered through a 100-μm filter (BD Biosciences, San Jose, CA), blocked, and incubated with fluorescent rat monoclonal antibodies against CD4 (PECy5, 1:330; eBioscience, San Diego, CA), CD8 (PE-Cy7, 1:100; eBioscience), F4/80 (FITC, 1:100, eBioscience), Gr1 (APC, 1:100; BD Biosciences), CD29 (AF700, 1:100; BioLegend, San Diego, CA), and CD45 (Pacific Blue, 1:200; Biolegend). Inflammatory macrophages and stromal fibroblast-like cells were gated as F4/80+Gr1+ double-positive and CD29+, respectively.[42,43] Appropriate isotype controls and unstained cells were used as controls. Cells were analyzed on a BD FACSAria cell sorter (BD Biosciences). Data were analyzed using FlowJo digital FACS software (Tree Star, Inc. Ashland, OR).

Quantitative polymerase chain reaction

On postinjury days 3 and 14, untreated wounds and hydrogel-treated wounds were harvested and total RNA was isolated using the RNeasy Fibrous Tissue Mini Kit (Qiagen, Valencia, CA) and reverse transcribed (Superscript First-Strand Synthesis kit; Invitrogen) using the following primers: vascular endothelial growth factor (VEGF), forward 5′-GGA GATCCTTCGAGGAGCACTT-3′ and reverse 5′-GGCGATT TAGCAGCAGATATAAGAA-3′; glyceraldehyde 3-phosphate dehydrogenase, forward 5′-TCAATGAAGGGGTCGTTGAT-3′ and reverse 5′-CGTCCCGTAGACAAAATGGT-3′. Real-time reactions were performed using SYBR Green PCR Master Mix (Qiagen) and the ABI Prism 7900HT Sequence Detection System (Applied Biosystems, Carlsbad, CA). VEGF expression was normalized to levels of glyceraldehyde 3-phosphate dehydrogenase as an internal control.

Statistical analysis

Microsoft Office Excel 2007 (Microsoft Corporation, Redding, WA) was used to perform unpaired *t*-test. Results are presented as mean ± standard error of the mean. A p-value <0.05 was considered statistically significant.

Results

Porous microarchitecture of hydrogel scaffolds

To control the porous microarchitecture of the pullulan hydrogel mixtures, we developed a novel phase-inversion technique to create open scaffold matrices. Hydrogel porosity was induced by addition of KCl salt. SEM analysis of hydrogels was performed immediately after the hydrogel dehydration step (Fig. 1). Crystalline structures were organized into various sized aggregates, which ranged in size from 10 to over 50 μm based on extrapolation of surface features (Fig. 1A–C). Analysis of 5% collagen–pullulan hydrogels demonstrated a diffuse and homogeneous distribution of collagen throughout the hydrogel based on collagen 1-specific immunostaining (Fig. 1E) and polarized light analysis of collagen fiber organization (Fig. 1F, G). Pullulan-based hydrogels fabricated without KCl displayed minimal porosity (Fig. 2A–C), whereas the addition of KCl resulted in a highly porous scaffold (Fig. 2D–F). Further, these crystalline structures were no longer seen following the salt dissolution steps, strongly suggesting a critical role for KCl crystallization in pore formation.

Pore characteristics were modulated by changing the amount of collagen added. Average pore sizes of 75.60 ± 2.16 μm, 34.15 ± 0.96 μm, and 15.70 ± 0.67 μm ($p < 0.05$) were calculated for 0%, 5%, and 10% collagen–pullulan hydrogels, respectively. Scaffold porosity was $\sim 82.4\% \pm 1.4\%$, $74.8\% \pm 2.6\%$, and $68.8\% \pm 1.8\%$ for hydrogels containing collagen at 0%, 5%, and 10%, respectively. Network extraction analysis revealed two-dimensional topographical similarities between the hydrogel porous ultrastructure (Fig. 3A–F) and the dermal collagen network of unwounded human dermal matrix (Fig. 3E, inset). The distributions of fiber length (Fig. 3G) and interfiber junctions (Fig. 3H) were most similar between the 5% collagen hydrogels and unwounded dermis, which prompted subsequent studies to be performed with the 5% collagen–pullulan hydrogels.

General physical properties

Hydrogels (5% collagen–pullulan) were durable, homogeneous, and could be easily handled. Dried hydrogel films were reproducibly cut into 6 mm disks of 2 mm thickness for all experiments. Incubation of dry disks in aqueous solution produced in a flexible and clear semirigid gel (Fig. 4A–C).

Hydrogel swelling

To investigate water retention properties, swelling studies were performed with water and PBS at different temperatures. Swollen hydrogels retained their general shape and did not degrade after overnight incubation in either deionized water (Fig. 4B) or PBS (Fig. 4C). Swelling ratios for 5% collagen–pullulan hydrogels incubated in deionized water at 4°C and 37°C were 19.92 ± 2.83 and 33.36 ± 7.97, respectively (Fig. 4D). Swelling ratios for 5% collagen–pullulan hydrogels incubated in PBS at 4°C and 37°C were 9.99 ± 1.47 and 9.27 ± 1.29, respectively (Fig. 4D). Hydrogel swelling did not significantly change between 12 and 72 h of incubation for all conditions, indicating maximal water absorption after overnight incubation.

Hydrogel degradation

To investigate the degradation profiles of the polymeric hydrogels, we performed enzymatic degradation studies. Incubation of 5% collagen–pullulan hydrogels with collagenase A (2 mg/mL) at room temperature resulted in scaffold degradation after 75 h. Pullulanase (4 U/mL) incubation resulted in scaffold degradation after 90 min. Combination

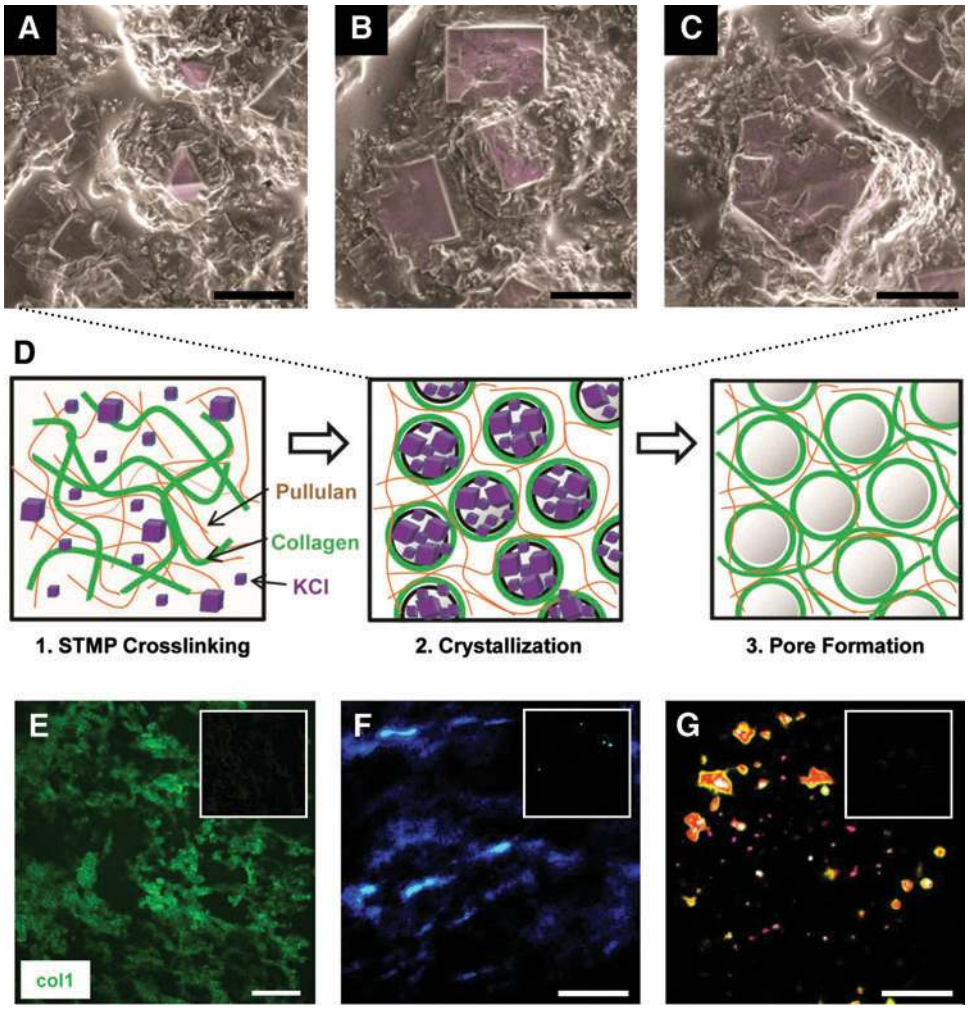

FIG. 1. Potassium chloride (KCl) crystallization and salt-induced phase inversion. After the dehydration processing step, scanning electron micrographs of 5% collagen–pullulan hydrogels demonstrated various KCl crystal sizes **(A–C,** pseudocolored purple**)** that correlated with hydrogel pore sizes produced after salt dissolution. We hypothesize that as water is rapidly removed from the hydrogel, localized supersaturation of KCl results in the formation of crystals around which polymers become organized **(D,** middle**)**. As KCl is dissolved from the hydrogel, porous macrovoids remain, resulting in a reticular pullulan–collagen composite scaffold **(D,** right**)**. The movement and organization of the polymers is further enhanced by mechanical mixing during the fabrication process **(D,** left**)**. Collagen 1 immunofluorescence demonstrates reticular and homogeneous distribution of collagen throughout the hydrogel **(E,** green = collagen 1**)**. Negative control shown in upper right inset **(E)**. Polarized light analysis of hydrogels **(F)** and picrosirius red-stained hydrogels **(G)** further confirms the homogeneous distribution of collagen around porous macrovoids throughout the hydrogel. The 0% collagen hydrogels shown in upper right inset of **(F)** and **(G)** demonstrate the absence of collagen signal. Scale bar for **(A–C)** is 10 μm. Scale bar for **(E–G)** is 100 μm. Color images available online at www.liebertonline.com/ten.

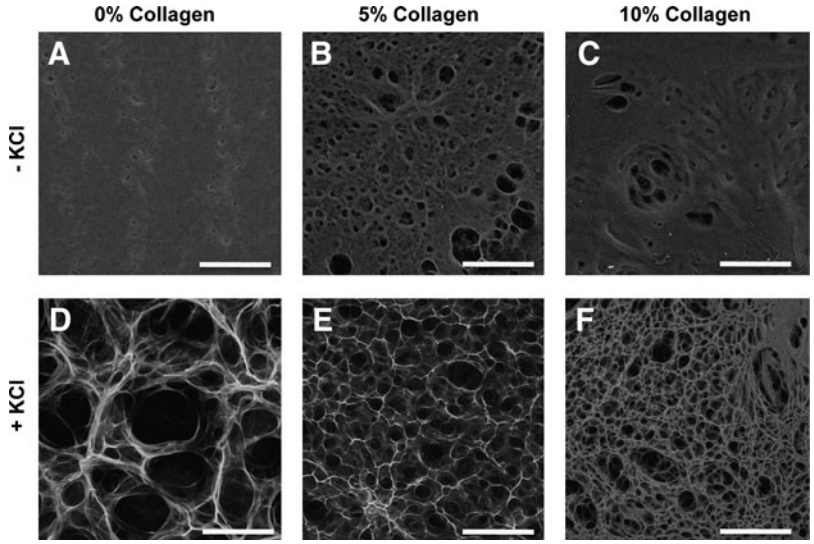

FIG. 2. Hydrogel pore formation. Scanning electron microscopy imaging revealed that pullulan hydrogels fabricated without KCl demonstrated poor porosity, despite increases in collagen content **(A–C)**. With the addition of KCl, consistent interconnected porous domains were created **(D–F)**. Alterations in collagen concentration significantly modified pore size. Scale bar is 100 μm.

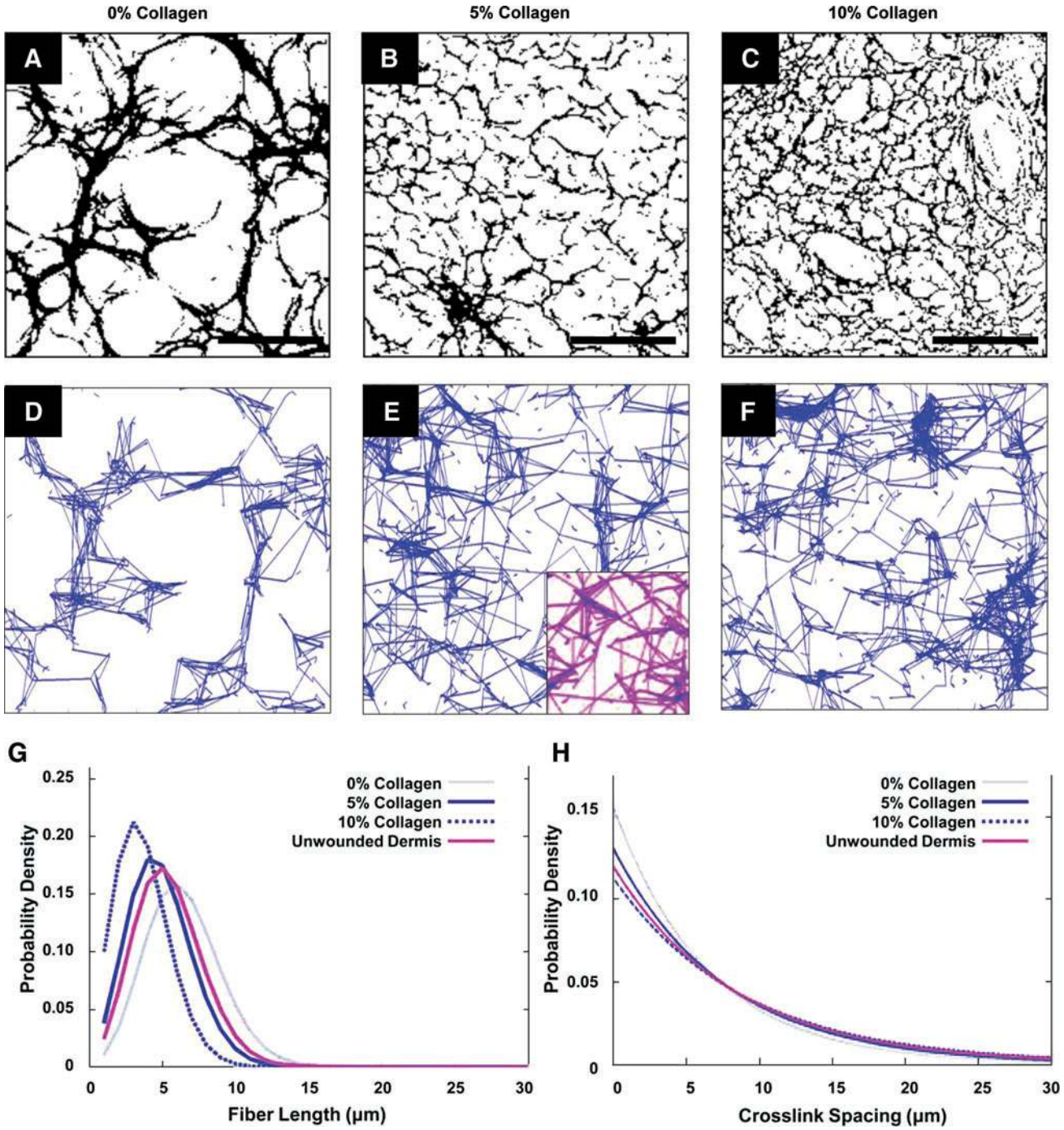

FIG. 3. Network extraction analysis. A network extraction algorithm was used to analyze the microstructure of pullulan-based hydrogels. Two-dimensional topographical data were extracted from representative scanning electron microscopy images for 0%, 5%, and 10% collagen–pullulan hydrogels **(A–F)**. The same algorithm was applied to acellular human dermal matrix **(E,** inset**)**. Quantitative analysis of fiber length **(G)** and crosslink spacing **(H)** distribution was performed, and 5% collagen hydrogel scaffolds (solid blue line) best approximated the microarchitecture of unwounded human dermis (purple line). Scale bar is 100 μm. Color images available online at www.liebertonline.com/ten.

degradation experiments resulted in hydrogel dissolution after 60 min (Fig. 5A).

Quantification of crosslinking

To understand the chemical interactions governing hydrogel stability, we examined crosslinking characteristics. Methylene blue binding was specific to STMP crosslinks as negative control mixtures without STMP demonstrated negligible binding (Fig. 5B). Collagen alone was also minimally crosslinked by STMP due to the paucity of free hydroxyl groups in collagen relative to pullulan. However, when collagen was added to pullulan, there was a significantly greater degree of STMP crosslinking compared with pullulan

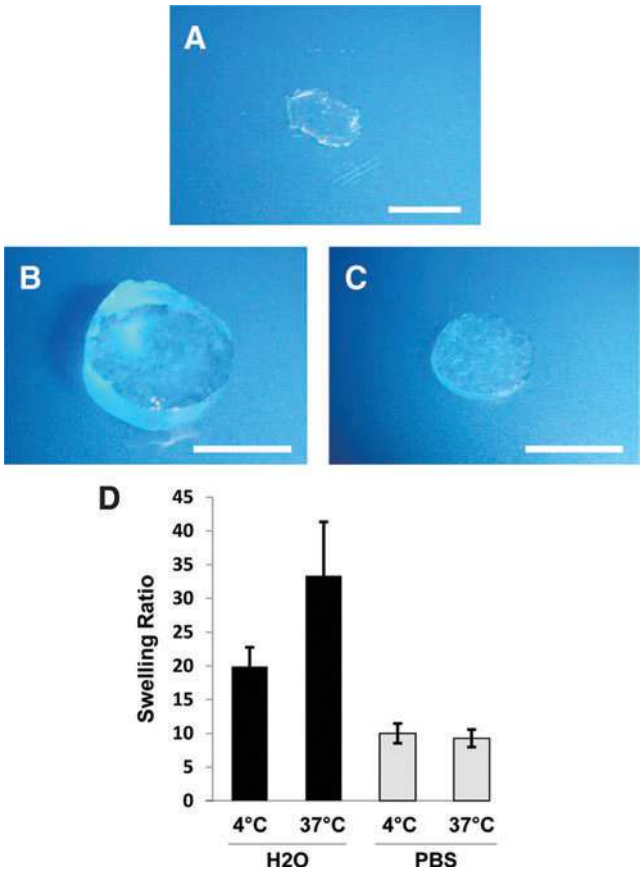

FIG. 4. Collagen–pullulan hydrogel general physical properties. Digital photographs of dry **(A)** and H_2O- **(B)** and phosphate-buffered saline (PBS)-incubated **(C)** 5% collagen–pullulan hydrogels after overnight incubation. Swelling ratios for 5% collagen–pullulan hydrogels were calculated after incubation in both dH_2O and PBS **(D)**. $n = 6$ for each condition. Error bars are ± standard error of the mean (SEM). Scale bar is 5 mm. Color images available online at www.liebertonline.com/ten.

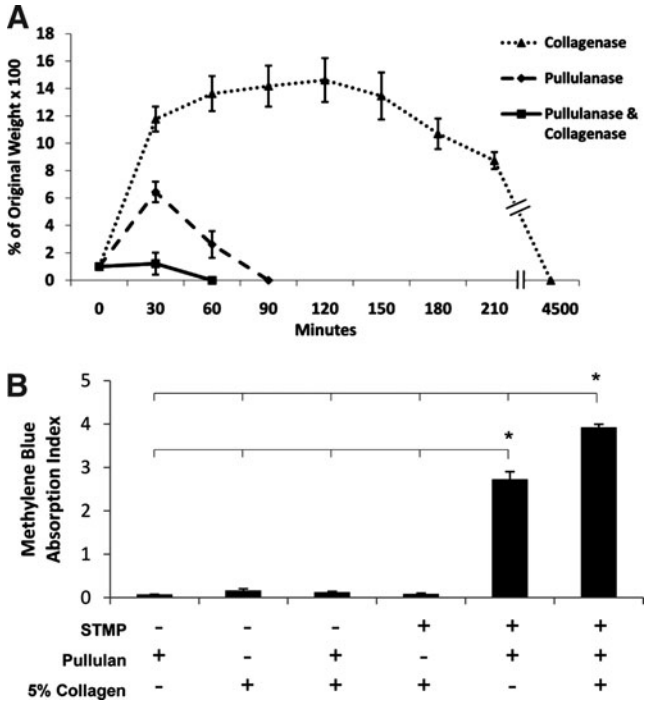

FIG. 5. Five percent collagen–pullulan hydrogel degradation and crosslinking. Hydrogels were incubated with pullulanase/collagenase (solid line), pullulanase only (dashed line), or collagenase only (dotted line) **(A)**. Five percent collagen without pullulan demonstrated minimal sodium trimetaphosphate (STMP) crosslinking based on methylene blue binding but appeared to synergistically augment the organization and crosslinking of pullulan hydrogels **(B)**. Polymer mixtures without STMP exhibited negligible nonspecific binding of methylene blue to either collagen or pullulan. $n = 6$ for each condition. Error bars are ± SEM. *$p < 0.05$.

and STMP alone (scaffold $AI_{MB} = 3.9$ for pullulan with 5% collagen vs. 2.7 for pullulan, $p < 0.05$), potentially through collagen-mediated hydrophobic interactions and synergistic promotion of pullulan organization.[44]

In vitro *viability and incorporation assays*

To assess hydrogel scaffold biocompatibility, we examined hydrogel viability with several cell types known to be involved in skin repair. Fibroblasts, MSCs, and endothelial cells exhibited over 97% viability over 7 days after seeding on 5% collagen–pullulan hydrogels, similar to control populations seeded without hydrogels (Fig. 6A–F). Fibroblasts and MSCs displayed successful invasion and attachment on SEM (Fig. 6G, H). These cellular invasion results confirm the interconnected open porous nature of the pullulan–collagen composite hydrogels.

Subcutaneous implantation of hydrogels

To examine *in vivo* characteristics of hydrogels, we performed subcutaneous implantation and excisional wound model experiments. All animals tolerated the surgical procedures well and all wounds showed no evidence of infection. Subcutaneous implant hydrogels demonstrated controlled degradation over 3 weeks (77.4% of original hydrogel area ± 6.9%, 41.9% ± 5.0%, 11.4% ± 2.6%, and 0% at days 3, 7, 14, and 21 postimplantation, respectively).

Excisional wound healing model

We next examined whether the hydrogel scaffold was capable of improving wound healing in a humanized wound model. Significant improvements in excisional wound closure were observed during early wound repair in hydrogel-treated wounds (Fig. 7A). The amount of wound closure was significantly greater in hydrogel-treated wounds compared with nontreated wounds at days 3 and 5 postinjury (86.4% original wound size ± 1.6% vs. 91.7% ± 1.0%, $p < 0.01$, and 59.4% ± 3.6% vs. 73.2% ± 2.5%, $p < 0.005$, respectively, Fig. 7B).

To examine possible mechanisms for the improvement in normal wound healing, we performed histologic analysis of wounds at postinjury days 3, 5, 7, and 14. At day 3, granulation tissue formation was significantly greater in hydrogel-treated wounds than in untreated wounds (122.67 ± 10.48 μm thickness vs. 63.69 ± 12.43 μm, $p < 0.01$, Fig. 8A, B, bracket). By day 5, this difference was no longer significant (100.14 ± 3.45 μm thickness in hydrogel-treated vs. 90.68 ± 8.51 μm in

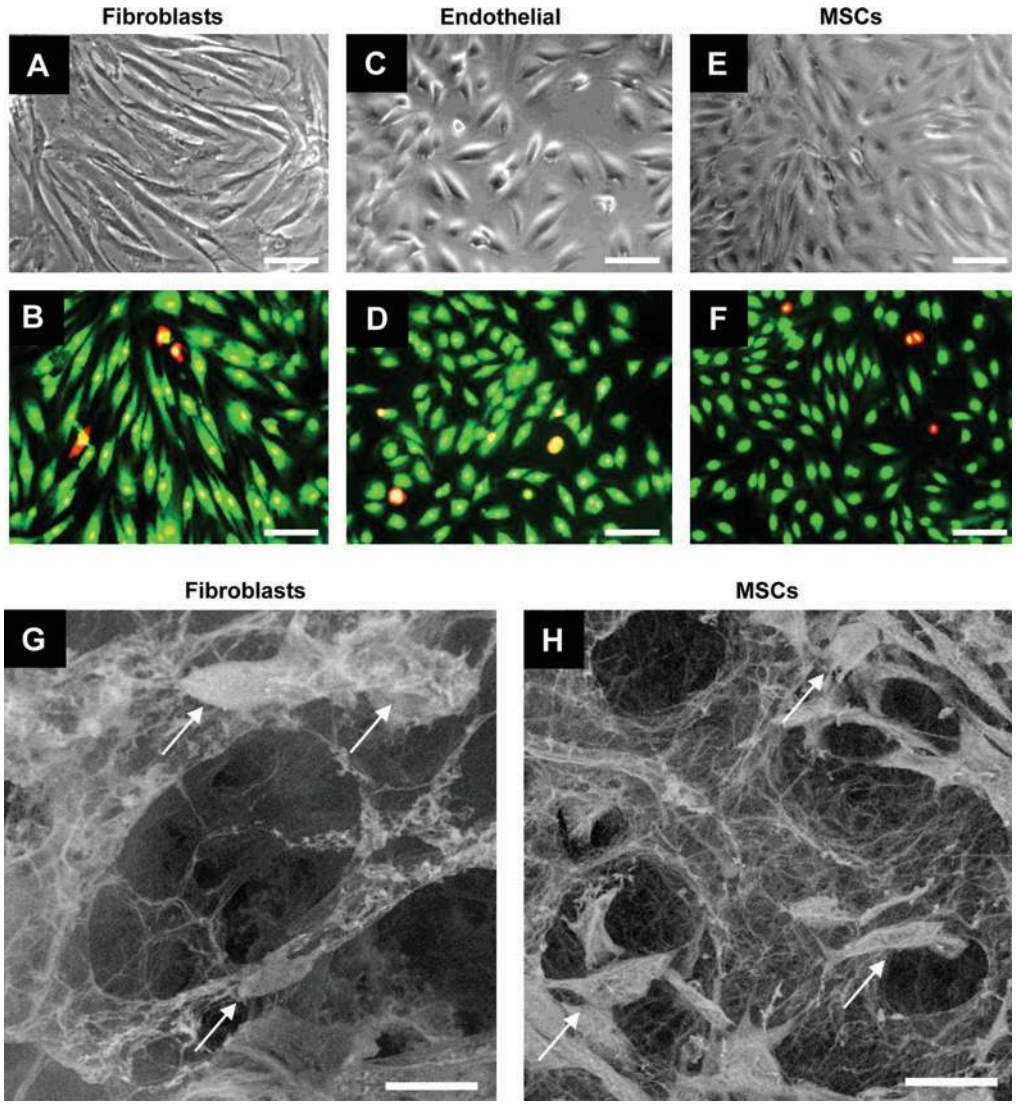

FIG. 6. *In vitro* cellular incorporation. Hydrogels were biocompatible with fibroblasts **(A, B)**, endothelial cells **(C, D)**, and bone marrow-derived mesenchymal stem cells (MSCs) **(E, F)** for up to 7 days. Live cells are stained green, whereas dead cells are stained red/yellow **(B, D, F)**. Scanning electron micrographs showed that both fibroblasts **(**arrows, **G)** and mesenchymal stem cells **(**arrows, **H)** were viably incorporated into 5% collagen–pullulan hydrogels. Additionally, the porous reticular network of the hydrogel scaffold is maintained in both images **(G, H)**. Scale bar is 50 μm in **(A–F)**. Scale bar is 25 μm in **(G)** and **(H)**. Color images available online at www.liebertonline.com/ten.

untreated, $p = 0.37$). As the granulation tissue remodeled into more mature dermis, there were no differences in dermal thickness between treated and untreated groups at days 7 and 14 postinjury. Keratinocytes were also observed to migrate over the dermal hydrogel (Fig. 8C, D), whereas the keratinocyte layer in nontreated excisional wounds was loosely maintained over a sparse granulation bed (Fig. 8E, F).

Flow cytometric analysis of wound cell populations

To characterize the specific cell populations within hydrogel-treated wounds versus nontreated wounds, we performed flow cytometric analysis of wound digests (Fig. 9A). At day 3, there was a significant increase in the recruitment of neutrophils (Gr1+, 48.58 ± 2.78 vs. 19.48 ± 2.88, $p < 0.001$), helper T cells (CD4+, 45.67 ± 2.75 vs. 16.42 ± 2.47, $p < 0.05$), and cytotoxic T cells (CD8+, 27.50 ± 1.87 vs. 13.69 ± 1.91, $p < 0.01$) with hydrogel treatment compared with untreated wounds. Recruitment of macrophages (F4/80+, 5.01 ± 0.81 vs. 9.98 ± 1.09, $p < 0.05$) and inflammatory macrophages (F4/80+Gr1+, 11.59 ± 1.38 vs. 19.42 ± 1.09, $p = 0.07$) was decreased at day 3 with hydrogel treatment compared with controls. Stromal-like cell recruitment (CD29+, 51.49 ± 2.74 vs. 27.44 ± 3.91, $p < 0.05$) was significantly increased with hydrogel treatment (Fig. 9B). These results demonstrate a potent hydrogel-induced immunomodulatory effect, which in aggregate may augment the recruitment of stromal-like cells capable of producing granulation matrix, consistent with our hematoxylin and eosin findings.

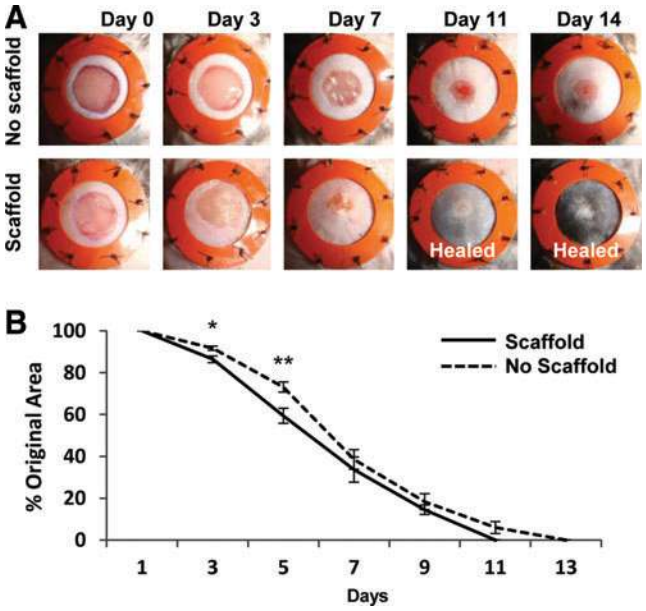

FIG. 7. Humanized excisional wound model. Digital photographs of stented excisional wounds treated with no scaffold (top row) or 5% collagen–pullulan scaffolds (bottom row) from days 0 to 14 postinjury **(A)**. The silicone rings prevent wound contraction and ensure that healing proceeds via granulation tissue formation and re-epithelialization, which is more similar to human healing. Five percent hydrogel scaffold-treated wounds demonstrated significantly improved wound closure at days 3 and 5 postinjury **(B)**. $n = 10$ wounds for each condition. Errors bars are $\pm$ SEM ($^*p < 0.01$ and $^{**}p < 0.005$). Color images available online at www.liebertonline.com/ten.

Analysis of matrix collagen and vascularity

To further characterize the formation of granulation tissue with hydrogel treatment, we performed trichrome staining and polarized light analysis of day 3 and day 14 wounds. Hydrogel treatment induced a significantly more robust and earlier granulation response (Fig. 9C, D) and areas of denser collagen production at day 14 postinjury (Fig. 9E–H). The enhanced formation of granulation tissue was also associated with increased induction of the cytokine VEGF (day 3 fold change 1.24 ± 1.04 compared with no hydrogel; day 14 fold change 4.53 ± 1.54, $p = 0.08$) and significantly elevated numbers of microvessels in the wound matrix (4.91 ± 0.75 microvessels per high-power field (hpf) vs. 2.25 ± 0.71 microvessels per hpf, $p < 0.05$) with hydrogel treatment compared to untreated controls (Fig. 9I, J).

Discussion

We have developed a method to fabricate modifiable dermal scaffolds that significantly improve normal wound healing in a humanized murine model. This technique is based on rapid desiccation of pullulan–collagen composite hydrogels through a salt-induced phase inversion process. We hypothesize that dehydration results in localized supersaturation and crystallization of KCl, similar to published studies demonstrating salt induction of micropore formation.[45] Scanning micrographs of rapidly dehydrated hydrogels demonstrated KCl crystals that correlated with the observed pore sizes seen after crystal dissolution. Collagen assembly is promoted around the crystals and throughout the hydrogel, resulting in an interconnected and homogeneously distributed collagen network after KCl dissolution. Although the diffusion of matrix elements through hydrogels has been described,[46] our fabrication technique also mechanically distributes the polymers throughout the hydrogel to promote the uniform organization of constituent polymers. To our knowledge, this is the first demonstration of KCl crystallization-induced pore formation applied to fabricate collagen scaffold hydrogels.

Bioengineered collagen scaffolds with pore sizes of 50–300 μm have previously been reported in the literature.[47–49] However, these data are mostly obtained from rigid scaffolds that can tolerate greater pore sizes without collapsing. Hydrogels inherently have less stiffness so larger pore sizes are difficult to achieve without risking collapse of the gel microstructure.[50] We hypothesized that 5% collagen hydrogels would be biocompatible despite a smaller average pore size given their swelling capacity, which allows for pore expansion in an exudative wound environment. Additionally, 5% collagen hydrogels best approximated the porous ultrastructure of human dermal matrix based on comparison of fiber length and crosslink distance using a network extraction analysis.[35,36]

Hydrogel-based biomaterials have demonstrated promising results for cutaneous wound healing. For example, chitosan hydrogels improved wound healing after burn injury in minipigs, but were applied as a topical gel and not associated with cellular or native matrix incorporation.[51] A gelable chitosan hydrogel was used to improve full-thickness excisional wound healing in mice, but the scaffold material was not highly integrated into the dermal wound.[52] Hyaluronan-based hydrogels augmented early collagen formation in a porcine injury model, but were not designed to recapitulate a porous dermal environment.[53] A new class of concentrated collagen hydrogels recently demonstrated improved biocompatibility *in vitro* and biologic integration *in vivo*, but these hydrogels were evaluated in a subcutaneous (non-dermal) environment,[54,55] somewhat limiting their relevance to dermal applications. In contrast to the previous studies, our pullulan-based hydrogel system effectively interfaced with the cutaneous wound, which permitted better evaluation of the translational relevance of this dermal construct. Further, the pullulan hydrogels recapitulated a porous dermal-like architecture both *in vitro* and *in vivo* and significantly augmented normal cutaneous wound repair, attributes not collectively demonstrated by any of the previous hydrogel systems. Taken together, these studies highlight the promising diversity of hydrogel systems for skin engineering, but of these hydrogel systems, only pullulan-based matrices were demonstrated to structurally mimic and articulate with the injured dermis while dramatically inducing granulation tissue formation.

Dermal scaffolds have also been engineered using combinations of collagen and glycosaminoglycans (GAG) such as chondroitin sulfate and hyaluronic acid.[56–61] Researchers have employed fabrication techniques, including lyophilization, electrospinning, and centrifugation, and crosslinking agents such as 1-ethyl-3-3-dimethylaminopropylcarbodiimide hydrochloride, *N*-hydroxysucinimide, and glutaraldehyde. As a class, these collagen–GAG scaffolds have demonstrated

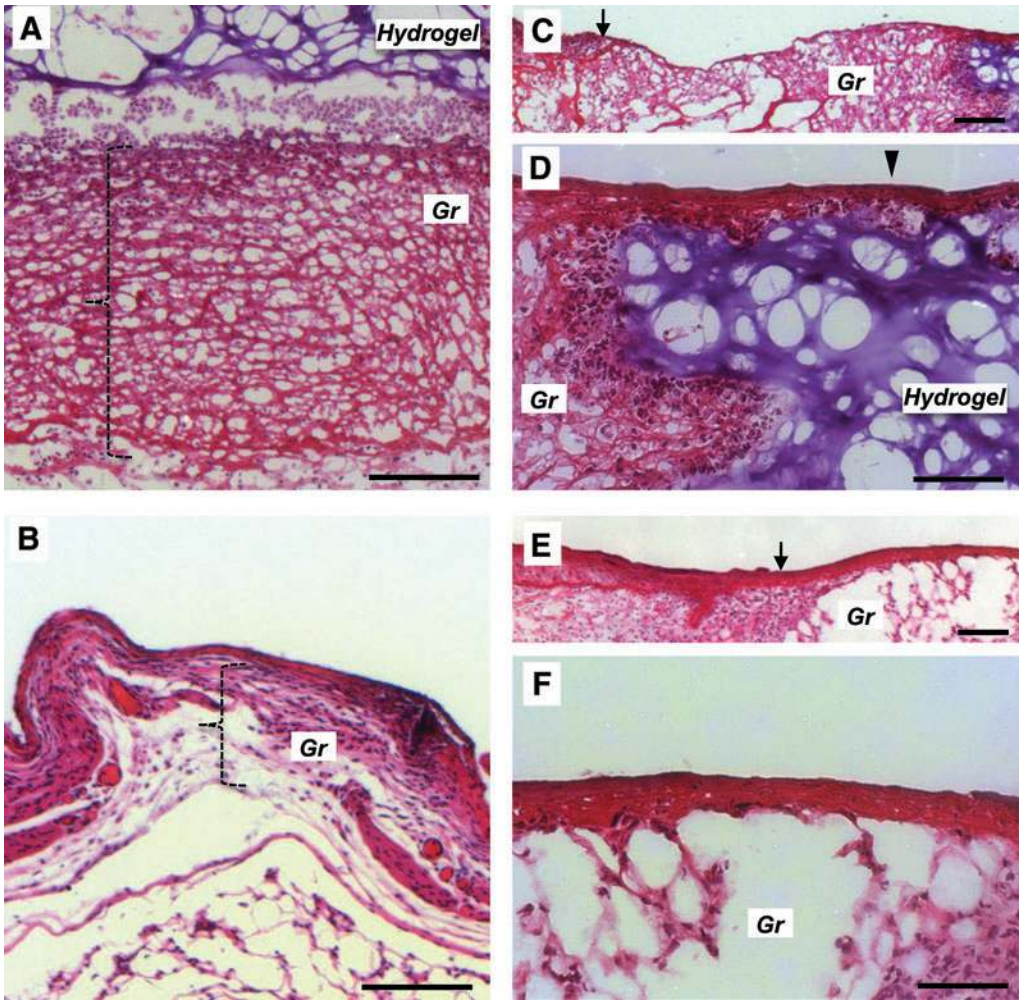

FIG. 8. Wound histology. Hematoxylin and eosin staining of day 3 hydrogel-treated excisional wounds (top series) compared with nontreated wounds (bottom series). Hydrogel-treated wounds demonstrated marked granulation (Gr) matrix formation **(A,** bracket**)** compared with thinner matrix in nontreated wounds **(B)**. A wide bed of granulation matrix is seen between the wound margin **(C,** arrow**)** and the hydrogel (purple staining). Layered keratinocytes are seen migrating across the wound bed over the hydrogel **(D,** arrowhead**)**. This is in contrast to nontreated excisional wounds, which demonstrate thinner granulation matrix **(B,** bracket**)** and sparse granulation tissue at the margin of the immature wound bed **(E,** arrow, and **F)**. Scale bar is 100 μm in **(A)** and **(B)** and 50 μm in **(C–F)**. Color images available online at www.liebertonline.com/ten.

excellent mechanical stability, porous architecture, and biocompatibility. For example, collagen–chondroitin sulfate–hyaluronic acid composite scaffolds improved wound healing in an open excisional wound model (similar to our murine study) in rats, but specific biologic mechanisms were not examined.[61] Although a study directly comparing collagen–GAG scaffolds and collagen–pullulan scaffolds is lacking, the successful fabrication of pullulan-based hydrogels using relatively simple and inexpensive materials shows that this technology may be yet another tool for skin engineers to create biomimetic dermal matrices.

Scanning micrographs showed that modulation of collagen concentration permitted regulation of pore size. It has been shown that collagen fibril formation is highly dependent on ionic interactions and pH,[62] both of which are influenced by KCl crystallization. With this hydrogel fabrication technique, we hypothesize that increasing the collagen concentration alters KCl crystal formation, which then affects subsequent pore size. Further, modulation of the concentration of collagen (which is dissolved in acetic acid) necessarily altered the pH environment during hydrogel fabrication and would have additionally influenced polymer organization within the hydrogel. Although surface SEM images were used to estimate bulk scaffold porosity, these findings were corroborated by histologic evaluation of sectioned hydrogels both *in vitro* and *in vivo*, demonstrating a highly interconnected porous architecture despite variations in collagen content. This relatively simple method to modulate pore characteristics can be exploited to create a variety of collagen-based scaffolds that can serve different biological functions.

The 5% collagen–pullulan scaffolds exhibit water retention and flexible hydrogel attributes that make them an attractive biomaterial for cell and small molecule delivery, providing a structured aqueous environment that is known to improve wound repair.[63] Composite 5% collagen–pullulan hydrogels were incubated in both water and PBS and exhibited swelling ratios ranging from 10 to 33. These data are consistent with previous studies on pullulan hydrogel hydration of

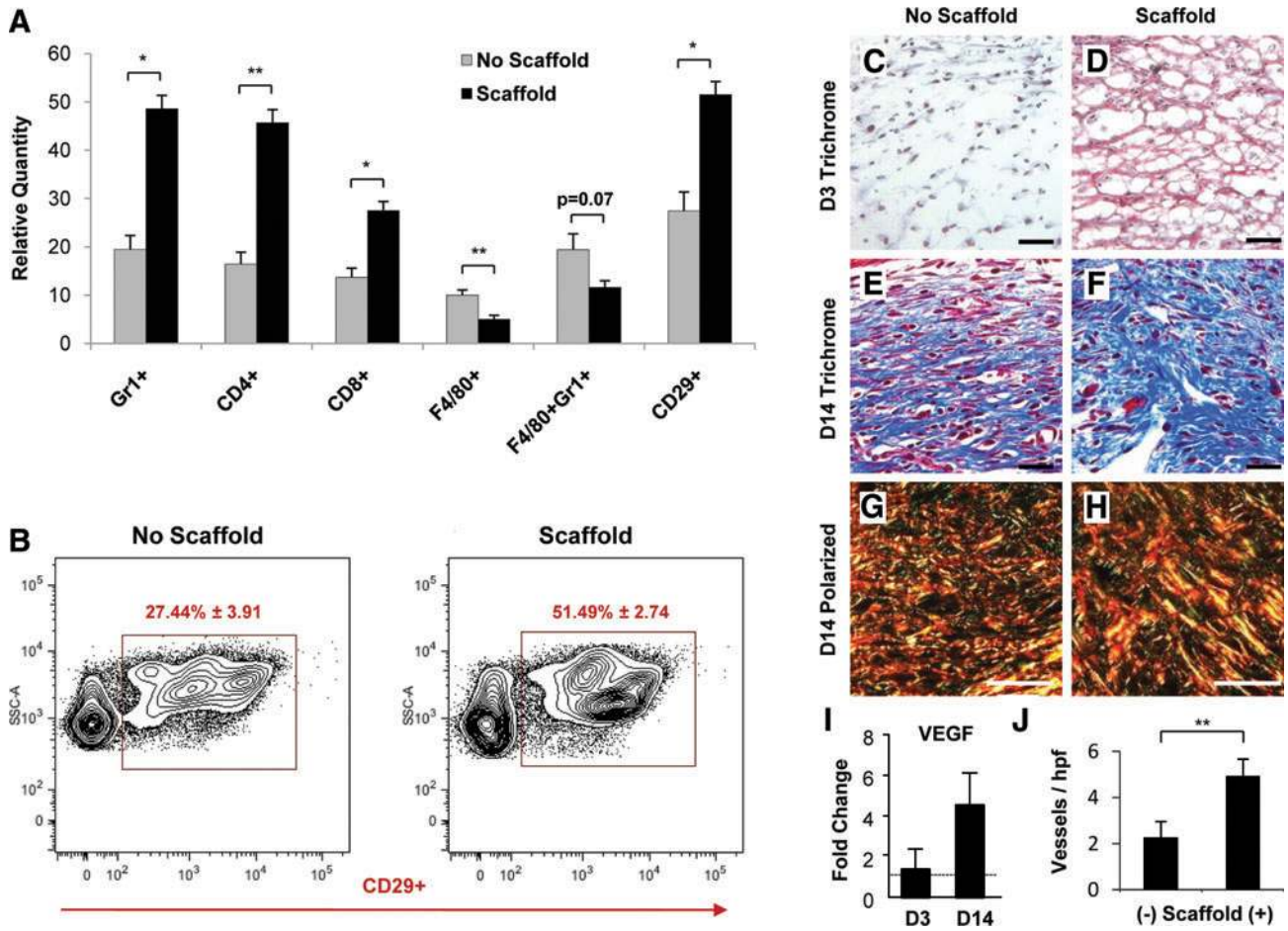

FIG. 9. Analysis of wound healing parameters. Flow cytometric analysis of wound cell populations at day 3 postinjury demonstrated increased recruitment of neutrophils and T cells and decreased recruitment of macrophage populations with hydrogel scaffold treatment **(A)**. Importantly, there was increased recruitment of stromal fibroblast-like CD29+ cells that are associated with granulation tissue formation and improved wound healing **(A)**. Representative flow cytometric graphs of CD29+ cell populations in control and hydrogel scaffold-treated wounds at day 3 postinjury **(B)**. $n = 4$ for each condition for flow cytometric analysis. Scaffold-treated wounds demonstrated improved granulation tissue formation based on trichrome and polarized light analysis compared with untreated controls **(C–H)**. Note the greater prevalence of mature collagen (blue on trichrome staining, red/orange on polarized light analysis) with hydrogel treatment at day 14 postinjury. Hydrogel treatment was also associated with greater gene expression of vascular endothelial growth factor (VEGF) and a significantly greater quantity of microvessels at day 14 postinjury **(I, J)**. Scale bar is 20 μm in **(C–H)**. Errors bars are ± SEM (*$p < 0.01$ and **$p < 0.05$). Color images available online at www.liebertonline.com/ten.

>90%[21] and swelling ratios of elastin-based hydrogels ranging from 18 to 33.[13] As expected, incubation with water resulted in greater swelling compared with PBS because of increased osmotic forces with hypotonic solutions. Increased swelling ratios at higher temperatures have also been shown with other hydrogels, attributed to disruption of secondary interactions and hydrogen bonds within polymers and facilitation of water absorption.[64]

Incubation of 5% collagen–pullulan hydrogels with both pullulanase and pullulanase/collagenase solutions resulted in rapid hydrogel dissolution. In contrast, incubation with collagenase alone did not result in rapid hydrogel degradation, suggesting that pullulan plays a major role in hydrogel stability. Methylene blue quantification of STMP crosslinking demonstrated that collagen may augment the organization of pullulan hydrogels through promoting hydrophobic interactions necessary for pullulan organization.[44] This predictable degradation profile can be employed to control encapsulated cell and/or ligand release via enzymatic methods. Additionally, the free hydroxyl groups can serve as highly modifiable side-groups for patterning of spatial cues, permitting precise control over the hydrogel scaffold microenvironment.

The structured aqueous nature of hydrogels provides an ideal environment for cellular growth and sustainability, as has been demonstrated with vascular cells,[21] chondrocytes,[65] and human MSCs.[66] *In vitro* studies performed with our engineered hydrogel scaffolds showed high biocompatibility and cellular incorporation with fibroblasts, MSCs, and endothelial cells. *In vivo*, we observed cellular infiltration, maintenance of hydrogel reticular architecture, and incorporation within the wound bed. The application of hydrogel scaffolds resulted in significant improvements during the early stages of normal wound healing, which we hypothesize

is due in part to its immunomodulatory effects on wound healing and collagen deposition.[67–69] The early increase in neutrophils and T lymphocytes was expected as part of an initial immune-mediated response to the biomaterial, but the attenuation of macrophage recruitment was an unexpected finding. Although macrophages are critical in wound repair, they may delay matrix deposition during the early phases of repair through their phagocytic and enzymatic activity.[42,70] CD29 expression has been associated with improved wound healing and may represent enhanced cell–cell and cell–matrix interactions mediated by hydrogel scaffold treatment.[43,71] This hydrogel-induced wound profile (recruitment of stromal fibroblast-like CD29+ cells coupled with reduced macrophage populations) may be critical for improved early wound repair and provides important insight into the active nature of biomaterial scaffold-based strategies.

Conclusions

Together, these data demonstrate that salt-induced phase inversion techniques can be used to fabricate highly modifiable dermal-like hydrogel scaffolds. This novel biomaterial recapitulates critical aspects of the structural context of unwounded skin both *in vitro* and *in vivo* and viably sustains cell populations necessary for normal skin repair. More importantly, we demonstrate an acceleration of normal wound healing, potentially by modifying cell recruitment and activation during acute inflammation and augmenting granulation tissue formation. Teleologically speaking, it has been thought that evolution has selected speed (rapid wound closure in the form of scar) over form (recapitulation of unwounded matrix), but future skin engineering strategies should strive to achieve both.

Acknowledgments

This project was supported by a grant to GCG from the United States Armed Forces Institute of Regenerative Medicine DOD #W81XWH-08-2-0032. M.G.G. was supported by a Howard Hughes Medical Institute Research Fellowship. The authors would like to thank Dr. Lydia-Marie Joubert for performing variable pressure SEM imaging, Ms. Yujin Park for histologic processing, and Mr. Ramalaxmareddy Kandimalla and Mr. Dean Nehama for assistance with hydrogel preparation.

Disclosure Statement

No competing financial interests exist.

References

1. Priya, S.G., Jungvid, H., and Kumar, A. Skin tissue engineering for tissue repair and regeneration. Tissue Eng B Rev **14,** 105, 2008.
2. Hodde, J.P., and Johnson, C.E. Extracellular matrix as a strategy for treating chronic wounds. Am J Clin Dermatol **8,** 61, 2007.
3. Bello, Y.M., Falabella, A.F., and Eaglstein, W.H. Tissue-engineered skin. Current status in wound healing. Am J Clin Dermatol **2,** 305, 2001.
4. Wainwright, D.J. Use of an acellular allograft dermal matrix (AlloDerm) in the management of full-thickness burns. Burns **21,** 243, 1995.
5. Gentzkow, G.D., Gidner, A., Davis, M., Kealey, G.P., Mozingo, D.W., and Hansbrough, J.F. Clinical trials of a biosynthetic temporary skin replacement, dermagraft-transitional covering, compared with cryopreserved human cadaver skin for temporary coverage of excised burn wounds. J Burn Care Rehabil **18,** 43, 1997.
6. Machens, H.G., Berger, A.C., and Mailaender, P. Bioartificial skin. Cells Tissues Organs **167,** 88, 2000.
7. Perumal, S., Antipova, O., and Orgel, J.P. Collagen fibril architecture, domain organization, and triple-helical conformation govern its proteolysis. Proc Natl Acad Sci U S A **105,** 2824, 2008.
8. Metcalfe, A.D., and Ferguson, M.W.J. Bioengineering skin using mechanisms of regeneration and repair. Biomaterials **28,** 5100, 2007.
9. Van Tomme, S.R., Storm, G., and Hennink, W.E. *In situ* gelling hydrogels for pharmaceutical and biomedical applications. Int J Pharm **355,** 1, 2008.
10. Khademhosseini, A., and Langer, R. Microengineered hydrogels for tissue engineering. Biomaterials **28,** 5087, 2007.
11. Schmidt, J.J., Rowley, J., and Kong, H.J. Hydrogels used for cell-based drug delivery. J Biomed Mater Research A **87,** 1113, 2008.
12. Kashyap, N., Kumar, N., and Kumar, M.N.V.R. Hydrogels for pharmaceutical and biomedical applications. Crit Rev Ther Drug Carrier Syst **22,** 107, 2005.
13. Annabi, N., Mithieux, S.M., Weiss, A.S., and Dehghani, F. The fabrication of elastin-based hydrogels using high pressure CO(2). Biomaterials **30,** 1, 2009.
14. Ahmed, T.A.E., Dare, E.V., and Hincke, M. Fibrin: a versatile scaffold for tissue engineering applications. Tissue Eng BRev **14,** 199, 2008.
15. Brandl, F., Sommer, F., and Goepferich, A. Rational design of hydrogels for tissue engineering: impact of physical factors on cell behavior. Biomaterials **28,** 134, 2007.
16. Leathers, T.D. Biotechnological production and applications of pullulan. Appl Microbiol Biotechnol **62,** 468, 2003.
17. San Juan Al, Hlawaty, H., Chaubet, F, Letourneur, D., and Feldman, L.J. Cationized pullulan 3D matrices as new materials for gene transfer. J Biomed Mater Res A **82,** 354, 2007.
18. Shingel, K.I. Current knowledge on biosynthesis, biological activity, and chemical modification of the exopolysaccharide, pullulan. Carbohydr Res **339,** 447, 2004.
19. Na, K., and Bae, Y.H. Self-assembled hydrogel nanoparticles responsive to tumor extracellular pH from pullulan derivative/sulfonamide conjugate: characterization, aggregation, and adriamycin release *in vitro*. Pharm Res **19,** 681, 2002.
20. Gupta, M., and Gupta, A.K. Hydrogel pullulan nanoparticles encapsulating pBUDLacZ plasmid as an efficient gene delivery carrier. J Controlled Release **99,** 157, 2004.
21. Autissier, A., Letourneur, D., and Le Visage, C. Pullulan-based hydrogel for smooth muscle cell culture. J Biomed Mater Res A **82,** 336, 2007.
22. Thebaud, N.-B., Pierron, D., Bareille, R., Le Visage, C., Letourneur, D., and Bordenave, L. Human endothelial progenitor cell attachment to polysaccharide-based hydrogels: a pre-requisite for vascular tissue engineering. J Mater Sci Mater Med **18,** 339, 2007.
23. Ambrosio, L., and Guarino, V. The synergic effect of polylactide fiber and calcium phosphate particle reinforcement in poly epsilon-caprolactone-based composite scaffolds. Acta Biomater **4,** 1778, 2008.

24. Feijen, J., Grijpma, D., and Hou, Q. Preparation of interconnected highly porous polymeric structures by a replication and freeze-drying process. J Biomed Mater Res B Appl Biomater **67,** 732, 2003.
25. Netti, P.A., Iannace, S., Di Maio, E., Oliviero, M., and Salerno, A. Design of porous polymeric scaffolds by gas foaming of heterogeneous blends. J Mater Sci Mater Med **20,** 2043, 2009.
26. Finne-Wistrand, A., Albertsson, A.-C., Kwon, O.H., Kawazoe, N., Chen, G., Kang, I.-K., *et al.* Resorbable scaffolds from three different techniques: electrospun fabrics, salt-leaching porous films, and smooth flat surfaces. Macromol Biosci **8,** 951, 2008.
27. Barbanti, S.H., Zavaglia, C.A.C., and Duek E.A.d.R. Effect of salt leaching on PCL and PLGA(50/50) resorbable scaffolds. Mater Res **11,** 75, 2008.
28. Heijkants, R.G.J.C., van Calck, R.V., van Tienen, T.G. de Groot, J.H., Pennings, A.J., Buma, P., *et al.* Polyurethane scaffold formation via a combination of salt leaching and thermally induced phase separation. J Biomed Mater Res A **87A,** 921, 2008.
29. Wunsch, E., and Heidrich, H. Determination of collagenase. Hoppe-Seyler Z Physiol Chem **333,** 149, 1963.
30. Dulong, V., Lack, S., Le Cerf, D., Picton, L., Vannier, J.P., and Muller, G. Hyaluronan-based hydrogels particles prepared by crosslinking with trisodium trimetaphosphate. Synthesis and characterization. Carbohydr Polym **57,** 1, 2004.
31. Lack, S., Dulong, V., Le Cerf, D., Picton, L., Argillier, J.F., and Muller, G. Hydrogels based on pullulan crosslinked with sodium trimetaphosphate (STMP): rheological study. Polym Bull **52,** 429, 2004.
32. Thangarajah, H., Vial, I.N., Chang, E., El-Ftesi, S., Januszyk, M., Chang, E.I., *et al.* IFATS series: adipose stromal cells adopt a proangiogenic phenotype under the influence of hypoxia. Stem Cells **27,** 266, 2009.
33. Joubert, L.M. Visualization of hydrogels with variable-pressure SEM. Microsc Microanal **15,** 1308, 2009.
34. Griffin, B.J. Variable pressure and environmental scanning electron microscopy: imaging of biological samples. Methods Mol Biol **369,** 467, 2007.
35. Stein, A.M., Vader, D.A., Jawerth, L.M., Weitz, D.A., and Sander, L.M. An algorithm for extracting the network geometry of three-dimensional collagen gels. J Microsc **232,** 463, 2008.
36. Wu, J., Rajwa, B., Filmer, D.L., Hoffman, C.M., Yuan, B., Chiang, C.S., *et al.* Automated quantification and reconstruction of collagen matrix from 3D confocal datasets. J Microsc **210,** 158, 2003.
37. Dikovsky, D., Bianco-Peled, H., and Seliktar, D. The effect of structural alterations of PEG-fibrinogen hydrogel scaffolds on 3-D cellular morphology and cellular migration. Biomaterials **27,** 1496, 2006.
38. Ferreira, L.S., Gerecht, S., Fuller, J., Shieh, H.F., Vunjak-Novakovic, G., and Langer, R. Bioactive hydrogel scaffolds for controllable vascular differentiation of human embryonic stem cells. Biomaterials **28,** 2706, 2007.
39. Galiano, R.D., Michaels, J., Dobryansky, M., Levine, J.P., and Gurtner, G.C. Quantitative and reproducible murine model of excisional wound healing. Wound Repair Regen **12,** 485, 2004.
40. Whittaker, P., Kloner, R.A., Boughner, D.R., and Pickering, J.G. Quantitative assessment of myocardial collagen with picrosirius red staining and circularly polarized light. Basic Res Cardiol **89,** 397, 1994.
41. Dolber, P.C., and Spach, M.S. Conventional and confocal fluorescence microscopy of collagen fibers in the heart. J Histochem Cytochem **41,** 465, 1993.
42. Daley, J.M., Brancato, S.K., Thomay, A.A., Reichner, J.S., and Albina, J.E. The phenotype of murine wound macrophages. J Leukoc Biol **87,** 59, 2010.
43. Hong, H.S., Lee, J., Lee, E., Kwon, Y.S., Ahn, W., Jiang, M.H., *et al.* A new role of substance P as an injury-inducible messenger for mobilization of CD29(+) stromal-like cells. Nat Med **15,** 425, 2009.
44. Na, K., Lee, E.S., and Bae, Y.H. Self-organized nanogels responding to tumor extracellular pH: pH-dependent drug release and *in vitro* cytotoxicity against MCF-7 cells. Bioconjug Chem **18,** 1568, 2007.
45. Lin, D.-J., Chang, C.-L., Huang, F.-M., and Cheng, L.-P. Effect of salt additive on the formation of microporous poly(vinylidene fluoride) membranes by phase inversion from LiClO4/Water/DMF/PVDF system. Polymer **44,** 413, 2003.
46. Shah, D.N., Recktenwall-Work, S.M., and Anseth, K.S. The effect of bioactive hydrogels on the secretion of extracellular matrix molecules by valvular interstitial cells. Biomaterials **29,** 2060, 2008.
47. George, J., Onodera, J., and Miyata, T. Biodegradable honeycomb collagen scaffold for dermal tissue engineering. J Biomed Mater Res A **87,** 1103, 2008.
48. Takemoto, S., Morimoto, N., Kimura, Y., Taira, T., Kitagawa, T., Tomihata, K., *et al.* Preparation of collagen/gelatin sponge scaffold for sustained release of bFGF. Tissue Eng A **14,** 1629, 2008.
49. Wang, H.J., Bertrand-De Haas, M., Riesle, J., Lamme, E., and Van Blitterswijk, C.A. Tissue engineering of dermal substitutes based on porous PEGT/PBT copolymer scaffolds: comparison of culture conditions. J Mater Sci Mater Med **14,** 235, 2003.
50. Chen, J., and Park, K. Synthesis and characterization of superporous hydrogel composites. J Controlled Release **65,** 73, 2000.
51. Boucard, N., Viton, C., Agay, D., Mari, E., Roger, T., Chancerelle, Y., *et al.* The use of physical hydrogels of chitosan for skin regeneration following third-degree burns. Biomaterials **28,** 3478, 2007.
52. Weng, L., Romanov, A., Rooney, J., and Chen, W. Non-cytotoxic, *in situ* gelable hydrogels composed of N-carboxyethyl chitosan and oxidized dextran. Biomaterials **29,** 3905, 2008.
53. Ghosh, K., Ren, X.-D., Shu, X.Z., Prestwich, G.D., and Clark, R.A.F. Fibronectin functional domains coupled to hyaluronan stimulate adult human dermal fibroblast responses critical for wound healing. Tissue Eng **12,** 601, 2006.
54. Helary, C., Abed, A., Mosser, G., Louedec, L., Meddahi-Pelle, A., and Giraud-Guille, M.M. Synthesis and *in vivo* integration of improved concentrated collagen hydrogels. J Tissue Eng Regen Med 2010, Jul 27 [Epub ahead of print].
55. Helary, C., Bataille, I., Abed, A., Illoul, C., Anglo, A., Louedec, L., *et al.* Concentrated collagen hydrogels as dermal substitutes. Biomaterials **31,** 481, 2010.
56. Pieper, J.S., Hafmans, T., Veerkamp, J.H., and van Kuppevelt, T.H. Development of tailor-made collagen-glycosaminoglycan matrices: EDC/NHS crosslinking, and ultrastructural aspects. Biomaterials **21,** 581, 2000.
57. Pieper, J.S., Oosterhof, A., Dijkstra, P.J., Veerkamp, J.H., and van Kuppevelt, T.H. Preparation and characterization of porous crosslinked collagenous matrices

containing bioavailable chondroitin sulphate. Biomaterials **20,** 847, 1999.
58. Pieper, J.S., van Wachem, P.B., van Luyn, M.J.A., Brouwer, L.A., Hafmans, T., Veerkamp, J.H., *et al.* Attachment of glycosaminoglycans to collagenous matrices modulates the tissue response in rats. Biomaterials **21,** 1689, 2000.
59. Liang, W.-H., Kienitz, B.L., Penick, K.J., Welter, J.F., Zawodzinski, T.A., and Baskaran, H. Concentrated collagen-chondroitin sulfate scaffolds for tissue engineering applications. J Biomed Mater Res A **94,** 1050, 2010.
60. Zhong, S., Teo, W.E., Zhu, X., Beuerman, R., Ramakrishna, S., and Yung, L.Y. Formation of collagen-glycosaminoglycan blended nanofibrous scaffolds and their biological properties. Biomacromolecules **6,** 2998, 2005.
61. Wang, W., Zhang, M., Lu, W., Zhang, X., Ma, D., Rong, X., *et al.* Cross-linked collagen-chondroitin sulfate-hyaluronic acid imitating extracellular matrix as scaffold for dermal tissue engineering. Tissue Eng C Methods **16,** 269, 2010.
62. Freudenberg, U., Behrens, S.H., Welzel, P.B., Muller, M., Grimmer, M., Salchert, K., *et al.* Electrostatic interactions modulate the conformation of collagen I. Biophys J **92,** 2108, 2007.
63. Field, C.K., and Kerstein, M.D. Overview of wound healing in a moist environment. Am J Surg **167,** S2, 1994.
64. Fang, J.-Y., Chen, J.-P., Leu, Y.-L., and Hu, J.-W. Temperature-sensitive hydrogels composed of chitosan and hyaluronic acid as injectable carriers for drug delivery. Eur J Pharm Biopharm **68,** 626, 2008.
65. Park, K.M., Joung, Y.K., Na, J.S., Lee, M.C., and Park, K.D. Thermosensitive chitosan-pluronic hydrogel as an injectable cell delivery carrier for cartilage regeneration. Acta Biomater **5,** 1956, 2009.
66. Keskar, V., Marion, N.W., Mao, J.J., and Gemeinhart, R.A. *In vitro* evaluation of macroporous hydrogels to facilitate stem cell infiltration, growth, and mineralization. Tissue Eng A **15,** 1695, 2009.
67. Delatte, S.J., Evans, J., Hebra, A., Adamson, W., Biemann Othersen, H., and Tagge, E.P. Effectiveness of beta-glucan collagen for treatment of partial-thickness burns in children. J Pediatr Surg **36,** 113, 2001.
68. Wei, D., Zhang, L., Williams, D.L., and Browder, I.W. Glucan stimulates human dermal fibroblast collagen biosynthesis through a nuclear factor-1 dependent mechanism. Wound Repair Regen **10,** 161, 2002.
69. Deters, A.M., Lengsfeld, C., and Hensel, A. Oligo- and polysaccharides exhibit a structure-dependent bioactivity on human keratinocytes *in vitro*. J Ethnopharmacol **102,** 391, 2005.
70. Gordon, S. Alternative activation of macrophages. Nat Rev Immunol **3,** 23, 2003.
71. Sasaki, M., Abe, R., Fujita, Y., Ando, S., Inokuma, D., and Shimizu, H. Mesenchymal stem cells are recruited into wounded skin and contribute to wound repair by transdifferentiation into multiple skin cell type. J Immunol **180,** 2581, 2008.

Address correspondence to:
Geoffrey C. Gurtner, M.D.
Department of Surgery
Stanford University School of Medicine
257 Campus Drive, GK201
Stanford, CA 94305

E-mail: ggurtner@stanford.edu

Received: May 19, 2010
Accepted: October 1, 2010
Online Publication Date: November 8, 2010